











**RESEARCH PAPER**

**Open Access**



# Wall-to-wall mapping of carbon loss within the Chernobyl Exclusion Zone after the 2020 catastrophic wildfire

Maksym Matsala<sup>1\*</sup> , Viktor Myroniuk<sup>1</sup> , Oleksandr Borsuk<sup>2</sup> , Denis Vishnevskiy<sup>2</sup> , Dmitry Schepaschenko<sup>3</sup> , Anatoly Shvidenko<sup>3</sup> , Florian Kraxner<sup>3</sup>  and Andrii Bilous<sup>1</sup> 

## Abstract

**Key message** We propose a framework to derive the direct loss of aboveground carbon stocks after the 2020 wildfire in forests of the Chernobyl Exclusion Zone using optical and radar Sentinel satellite data. Carbon stocks were adequately predicted using stand-wise inventory data and local combustion factors where new field observations are impossible. Both the standalone Sentinel-1 backscatter delta (before and after fire) indicator and radar-based change model reliably predicted the associated carbon loss.

**Context** The Chernobyl Exclusion Zone (CEZ) is a mosaic forest landscape undergoing dynamic natural disturbances. Local forests are mostly planted and have low ecosystem resilience against the negative impact of global climate and land use change. Carbon stock fluxes after wildfires in the area have not yet been quantified. However, the assessment of this and other ecosystem service flows is crucial in contaminated (both radioactively and by unexploded ordnance) landscapes of the CEZ.

**Aims** The aim of this study was to estimate carbon stock losses resulting from the catastrophic 2020 fires in the CEZ using satellite data, as field visitations or aerial surveys are impossible due to the ongoing war.

**Methods** The aboveground carbon stock was predicted in a wall-to-wall manner using random forest modelling based on Sentinel data (both optical and synthetic aperture radar or SAR). We modelled the carbon stock loss using the change in Sentinel-1 backscatter before and after the fire events and local combustion factors.

**Results** Random forest models performed well (root-mean-square error (RMSE) of 22.6 MgC·ha<sup>-1</sup> or 37% of the mean) to predict the pre-fire carbon stock. The modelled carbon loss was estimated to be 156.3 Gg C (9.8% of the carbon stock in burned forests or 1.5% at the CEZ level). The standalone SAR backscatter delta showed a higher RMSE than the modelled estimate but better systematic agreement (0.90 vs. 0.73). Scots pine (*Pinus sylvestris* L.)-dominated stands contributed the most to carbon stock loss, with 74% of forests burned in 2020.

**Conclusion** The change in SAR backscatter before and after a fire event can be used as a rough proxy indicator of aboveground carbon stock loss for timely carbon map updating. The model using SAR backscatter change and backscatter values prior to wildfire is able to reliably estimate carbon emissions when on-ground monitoring is impossible.

**Keywords** Chernobyl forest, Sentinel, Carbon emissions, Synthetic aperture radar, Multispectral satellite data

Handling editor: Shengli Tao

\*Correspondence:

Maksym Matsala

[matsala@nubjp.edu.ua](mailto:matsala@nubjp.edu.ua)

Full list of author information is available at the end of the article



© The Author(s) 2023. **Open Access** This article is licensed under a Creative Commons Attribution 4.0 International License, which permits use, sharing, adaptation, distribution and reproduction in any medium or format, as long as you give appropriate credit to the original author(s) and the source, provide a link to the Creative Commons licence, and indicate if changes were made. The images or other third party material in this article are included in the article's Creative Commons licence, unless indicated otherwise in a credit line to the material. If material is not included in the article's Creative Commons licence and your intended use is not permitted by statutory regulation or exceeds the permitted use, you will need to obtain permission directly from the copyright holder. To view a copy of this licence, visit <http://creativecommons.org/licenses/by/4.0/>.

## 1 Introduction

A disaster at the Chernobyl (Chernobyl) Nuclear Power Plant in northern Ukraine (1986) was ranked as the second largest (after the Bhopal tragedy, India, 1984) technogenic catastrophe in human history (Tikhomirov & Scheglov 1994). A substantial amount of long- and medium-lived artificial radionuclides were deposited in the surrounding natural environment and across human-modified landscapes such as croplands (Evangelidou et al. 2016). A distinct area around the Chernobyl Nuclear Power Plant encompassing abandoned farmlands and planted forests affected by high radioactive contamination rates was set aside as the Chernobyl Exclusion Zone (CEZ) (Yoschenko et al. 2017). Highly limited silviculture and uncontrolled natural succession across former croplands accelerated the transition of the CEZ area to a complex mosaic of forest and non-forest vegetation, with spatial aggregations of homogeneous planted forest and heterogeneous naturally vegetated patches. In the last decade, this complex landscape configuration has been dynamically shaped by multiple wildfire events (Beresford et al. 2021).

Wildfires are among the most important agents of natural forest disturbances in regions such as Fenno-Scandia (Clear et al. 2014), Central Europe (Neumann et al. 2022), Northern Asia (Feurdean et al. 2020), Australia (Tran et al. 2020), and Pacific North America (Halofsky et al. 2020). The extent, frequency, and severity of these fires are increasing under global climate change (Zheng et al. 2021). In Ukraine, a majority of wildfires are caused by humans: the practice of illegal stubble grass burning by farmers remains the main reason for ignitions (Ager et al. 2019). Due to access restrictions and the low density of the human population in the vicinity of the CEZ, the area is prone to catastrophic fire events. Scots pine (*Pinus sylvestris* L.) forests represent a typical Soviet-era legacy when even-aged monocultures were perceived by conventional forest regeneration practices as the only possible option, disregarding changes in socio-economic and ecological conditions (Shvidenko et al. 2017). Lack of conventional forest management (i.e. absence of silvicultural treatments such as regular thinning and dead wood removal) in these forests led to accumulation of fuels, thus increasing the risk of ignitions and the rate of spread of wildfires occurring near CEZ borders (Matsala et al. 2021b).

Wildfires cause increased carbon emissions (loss to the atmosphere) from forests due to direct burning of biomass (tree foliage, understorey, litter, partial consumption of standing live and dead trees, downed tree boles, and small branches) and indirectly by causing mortality of damaged trees that emit carbon via decomposition. A number of empirical and modelling approaches exist

to account for carbon emissions during forest wildfires (Gerrand et al. 2021). Methods based on remote sensing (satellite), mostly using optical bands, are frequently applied across the globe for that purpose (Cruz-Lopez et al. 2019; Gale and Cary 2022). This type of data, however, only partially represents forest biomass compartments (stem and crown biomass visible from above). That is, only indirect estimation can be made for understorey biomass compartments using a correlation from allometric relationships between growing stock volume and understorey.

Delta (difference) of the normalized burn ratio (NBR) index based on optical infrared band values is the most frequently applied remote-sensing indicator of wildfire severity (e.g. Tran et al. 2018; Sannigrahi et al. 2020). Additionally, it was extensively used to derive biomass change estimates (including loss caused by natural and human disturbances) extracted from temporal segmentation algorithm outputs (Nguyen et al. 2020). Another common approach is to assign empirical combustion factors (percent of biomass compartment typically lost during burning) to pre-fire biomass stock estimates (e.g. Volkova et al. 2019; 2022). However, NBR reflects only spectral changes and cannot fully address biomass loss, as, inter alia, dead trees continue to store carbon. Backscatter satellite data acquired by synthetic aperture radar (SAR) spacecraft have shown an additional capacity to characterize changes in forest structure and biomass stocks (Tanase et al. 2019; Bruggiser et al. 2021). In contrast to optical satellite data, it captures the differences in the textural sharpness of the surface. That is, trees killed by fire with burned canopies are assumed to reflect slightly less microwave backscatter (fewer leaves and twigs decrease the volume scattering effect), while the relative spectral loss expressed by delta NBR is assumed to be higher and tends to overestimate the real instant carbon loss (Tanase et al. 2015). The combination of these types of satellite data has become extremely efficient with the launch of the Sentinel-2 mission (2015) in addition to Sentinel-1 SAR spacecrafts (2014).

Dense time series of satellite imagery provide a robust background to fit spatially explicit statistical models of biomass or carbon stocks. Recent studies have shown that reliable biomass estimates over time can also be achieved using a single-date inventory of forest attributes (needed to calculate carbon storage, Nguyen et al. 2020). This is crucial for carbon inventories in the CEZ, which is characterized by a dynamically changing environment and has limited human access due to radioactive contamination. The Russian military invasion of 2022 caused new restrictions on visits to the area near the state border of Ukraine (including the CEZ) and on any aerial data acquisitions to monitor burned sites. Thus, we attempted

to estimate carbon loss from forest ecosystems following the largest CEZ wildfire that burned in 2020 based on a single-date forest inventory (2016), local forest biomass combustion factors, and satellite data from the Sentinel time series. We relied on the post-fire change in Sentinel-1 backscatter instead of the difference in the optical range of the electromagnetic spectrum (e.g. delta NBR) to minimize possible carbon loss overestimation. That is, we suggest that the delta of radar backscatter can more comprehensively capture the change in carbon stock in the main biomass compartment — stemwood. Our specific objectives were two-fold: (1) to map carbon stocks using both optical and SAR Sentinel imagery and (2) to compare modelling approaches estimating relative carbon loss (%) after the 2020 wildfire using two approaches. The first approach is based on the standalone Sentinel-1 backscatter delta predictor, which simply depicts the difference between pre- and post-fire Sentinel-1 imagery. The second approach is based on the regression model that fits the carbon loss using four Sentinel-1 predictors (two pre-fire backscatter indicators and their post-fire delta). We believe this mapping effort may uncover the paramount importance of SAR satellite data to derive accurate and cost-effective estimates of forest carbon change after catastrophic fires in regions with similar biogeographic conditions.

## 2 Material and methods

### 2.1 Study area and local fire regime

The CEZ, with an area of 2600 km<sup>2</sup>, was set aside after the 1986 nuclear disaster in northern Ukraine. The CEZ was formed to encompass the forests with the highest level of contamination by <sup>137</sup>Cs, <sup>90</sup>Sr, and transuranium elements (Tikhomirov & Scheglov 1994). The CEZ territory is represented by a portion of the Eastern European Plain (elevation does not exceed 200 m above sea level) with low, swampy left and high right banks of the Prypiat River. The main area on the right bank of the Prypiat River is covered by forests and abandoned croplands reverting to forest. The dominant local tree species are Scots pine, silver birch (*Betula pendula* Roth.), black alder (*Alnus glutinosa* (Gaertn.) L.), and European oak (*Quercus robur* L.).

The tree cover in the CEZ according to remote-sensing data was 41% in 1986 (Matsala et al. 2021a) and reached 59% in 2020. Forest management activities were strictly limited, and agricultural activities were fully prohibited. The absence of thinning has largely contributed to fuel accumulation (Ager et al. 2019) and therefore to the occurrence of catastrophic wildfires.

The recent catastrophic wildfire in April 2020 was ignited outside the western border of the CEZ. Fire moved through young forest regrowth and dead wood accumulated after the 2015 wildfire to mature Scots

pine forests in the central part of the CEZ. Other fire events (in April 2020) were located south of the Chornobyl Nuclear Power Plant, in the southern part of the CEZ, and on the left bank of the Prypiat River. In total, the 2020 wildfire burned ~38,000 ha of forest in the CEZ (Fig. 1).

### 2.2 Forest attribute training and validation data

The main source of training data for the regression model of carbon stocks was a dataset of forest polygons inventoried in 2016 (Fig. 2). Each polygon (~40,000 in total) represented a distinct forest patch with common forest characteristics and tree species composition. Mean stand characteristics within each polygon were defined by visual inspection by trained members of inventory crews by calipering tree diameters at breast height (DBH) and measuring heights of selected trees using altimeters.

We randomly sampled two stratified datasets from the CEZ forest polygon dataset: one for the calibration of the carbon stock model and another for the validation of model performance. Both datasets were stratified by a combination of stand age and main tree species in a stand (Table 1).

Each sample group (Table 1) contained 381 polygons to train the model and 205 polygons for validation. The number of 'model training' polygons was defined to obtain a 95% confidence level with a 5% margin of error associated with a total 'population' of 40,000 (total number of polygons). The number of 'validation' polygons was defined under the same conditions but with a 7% margin of error.

Forest attributes for each polygon (mean stand DBH, average tree height, relative stocking (value between 0 and 1), site index (according to the Ukrainian encoding system), stand age, and dominant tree species) were used to calculate the size of biomass compartments and carbon stocks.

### 2.3 Carbon estimation

We approximated the biomass (both live and dead) stocks for all sample groups using allometric models described in Bilous et al. (2017), Lakyda et al. (2019), and Myroniuk et al. (2020). Biomass stocks were calculated based on forest polygon attributes for aboveground live (stems outside bark, tree branches and foliage, understorey, green forest floor) and dead (snags, logs, fine litter, and coarse ( $d > 1$  cm) branches) biomass. The carbon content was assumed to be 50% of the biomass, except for crown foliage, understorey, green forest floor (49%), and fine litter (37%).

The calculated carbon stocks for all biomass compartments were summed to derive the total estimates used in model training and validation.

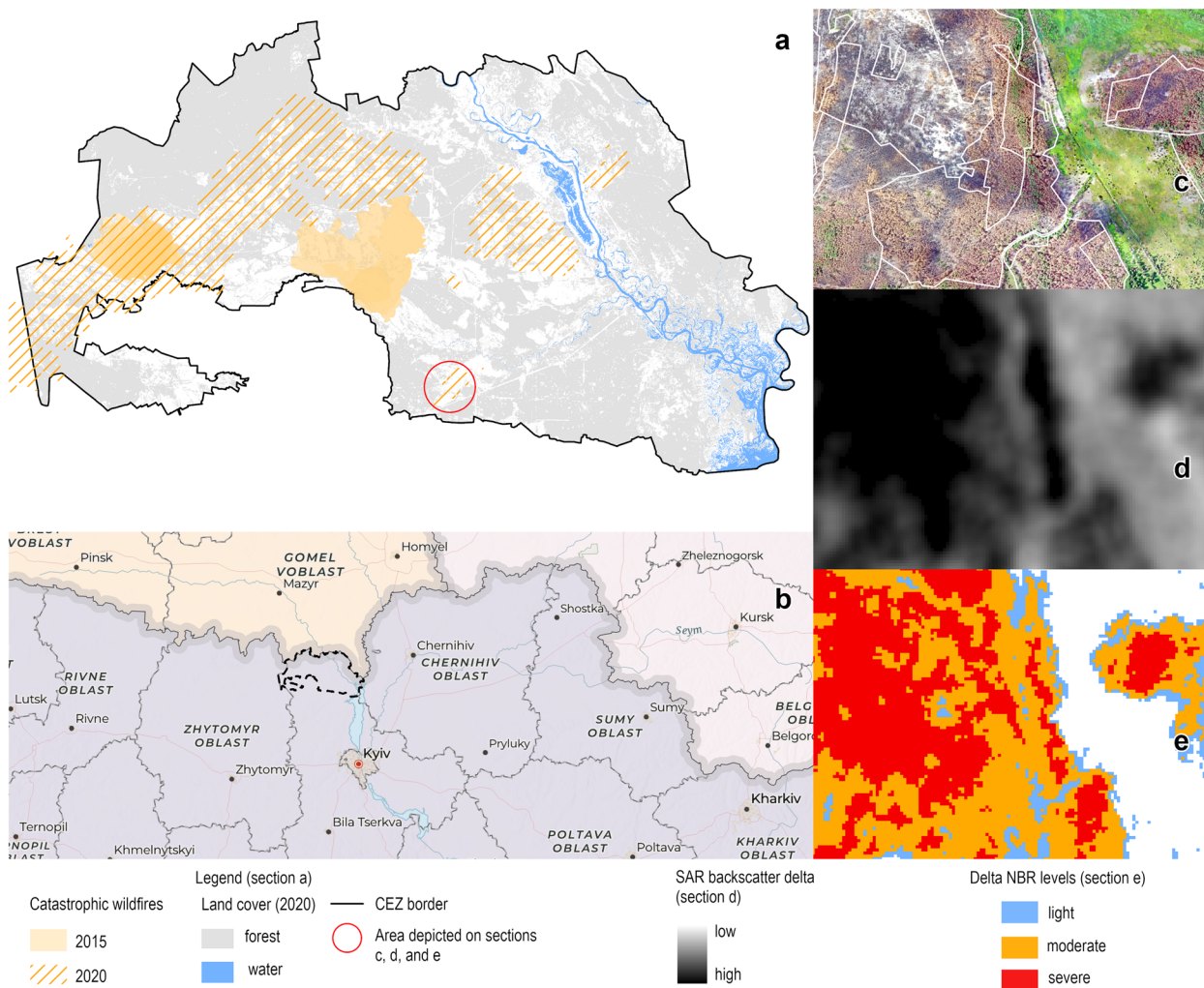


**Fig. 1** Chornobyl Exclusion Zone (CEZ) with forest mask (grey, as for 2020 based on Matsala et al. (2021b)) and fire perimeters (orange, **a**). The black dashed line shows the CEZ boundary at a larger geographical scale (**b**). Aerial image acquired over the example part of the study area (marked by a red circle on **a**) (**c**). Delta of Sentinel-1 backscatter of VH polarization for the example part of the study area (**d**). Delta NBR levels for the example part of study area (**e**)

### 2.4 Remote-sensing data and regression carbon stock model

We used the median composites of Sentinel-1 and Sentinel-2 images acquired during the on-leaf season (25 April – 25 September) in 2016. We used the top-of-atmosphere reflectance multispectral images because the surface reflectance data were available only starting in April 2017. Multispectral variables from cloudless median composites included three visible (red, green, blue), near-infrared (NIR), four red-edge, and two shortwave-infrared band values. Additionally, the normalized difference vegetation index (NDVI) based on NIR and red values was computed. Radar variables included backscatter values at two polarizations of Sentinel-1 C-band ground range detected data:

vertical–vertical (VV) and vertical-horizontal (VH) converted to decibels. These two datasets were corrected on the Google Earth Engine platform (thermal noise removal, radiometric calibration, and terrain correction). Then, radar datasets were filtered with a Lee speckle filter. In total, 13 variables were used to calibrate the carbon stock random forest (RF, Breiman 2001) model.

We also tested alternative predictor combinations: ‘visible’ and infrared predictors, ‘visible’ and Sentinel-1 backscatter predictors, and two standalone Sentinel-1 backscatter predictors. The first combination (‘visible’ and infrared predictors) represents a classic option when only optical data are available. The second combination is designed based on our assumption that infrared band values can underestimate carbon in burned



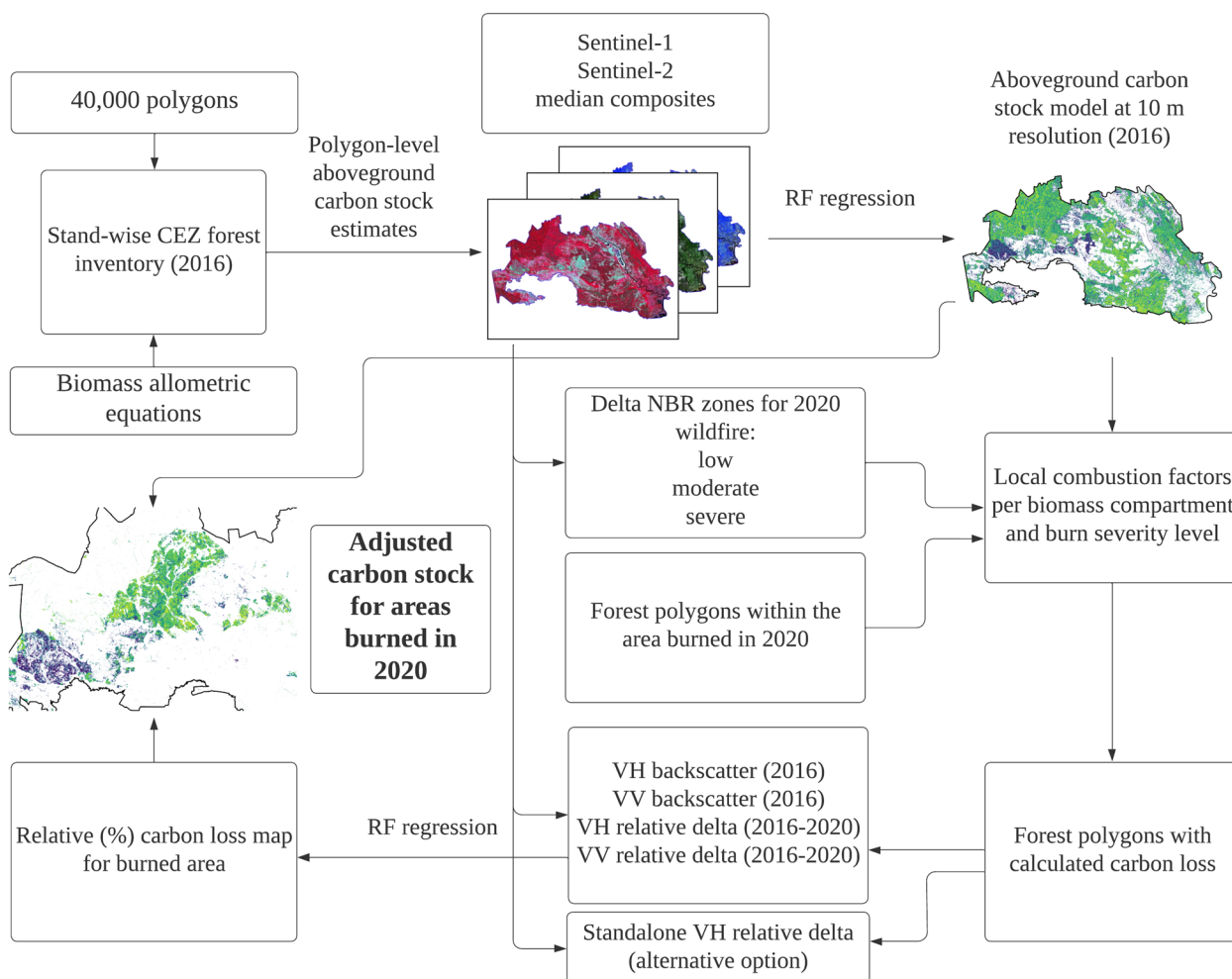


**Fig. 2** General workflow of the study. Stand-wise CEZ forest inventory data and Sentinel satellite imagery are used to predict the aboveground carbon stock for 2016. Then, the forest area burned in 2020 is defined using delta NBR zones. Post-fire carbon on training forest polygons is calculated by applying local combustion factors. The relative carbon loss is derived using the stand-alone delta of backscatter at VH polarization or based on the model calibrated with four SAR-based predictors

**Table 1** Stratification of training and validation data on forest attributes

Sample group	Stand age, year
Young Scots pine	1–40
Middle-aged Scots pine	41–80
Mature Scots pine	>80
Young silver birch	1–20
Middle-aged silver birch	21–50
Mature silver birch	>50
Young and middle-aged black alder	1–40
Mature black alder	>40
European oak	Any
Common aspen ( <i>Populus tremula</i> L.)	Any

areas (as standing dead trees without foliage — snags — severely lack chlorophyll content to reflect in infrared part of the electromagnetic spectrum), and ‘visible’ and Sentinel-1 backscatter predictors could predict total aboveground carbon with lower bias. The third option was used to understand how forest carbon stocks could be predicted ignoring the optical characteristics of tree species and chlorophyll content at all.

The model was trained based on explanatory variables extracted from the median Sentinel-1 and Sentinel-2 composites. The RF model was run with default hyperparameters: the number of decision trees in an ensemble was 500, and the number of variables selected at each decision tree split was a square root of the number of variables, i.e.  $\sqrt{13}$ . The RF approach was chosen among different machine learning methods because it is fast, produces reliable outputs without long hyperparameter

tuning, and returns the relative importance of model variables based on the increase in model errors if excluding such variables from the set.

We estimated the performance of the carbon stock RF regression model based on the root-mean-square error (RMSE) and its relative value (% to the mean of a sample). Additionally, an agreement coefficient (AC) was calculated based on geometrical mean functional regression (GMFR) between the observed and predicted values (Ji & Gallo 2006; Riemann et al. 2010). GMFR is a symmetric regression function where both observed and predicted values could be a source of error. According to Riemann et al. (2010), it is used to derive a systematic and unsystematic difference. The systematic agreement coefficient ( $AC_{sys}$ ) shows the difference between the 1:1 line and the GMFR fit. The unsystematic agreement coefficient ( $AC_{uns}$ ) shows a variation in the data points around the GMFR fit. AC is a product of  $AC_{sys}$  and  $AC_{uns}$ ; all three metric values range between 0 and 1, with 0 indicating a lack of agreement and 1 representing full agreement. All performance metrics were computed for the validation sample polygon dataset (for 2016), which was not used in model calibration.

The model was calibrated in the R environment, and raster data were downloaded from the Google Earth Engine platform (Gorelick et al. 2017).

### 2.5 Carbon loss modelling

We modelled carbon loss in four steps. First, we extracted burned areas from Sentinel-2 composites using the change in NBR values (delta NBR) between 2020 and 2019. Burned areas were then classified into three discrete levels of fire severity outlined in Key and Benson (2006) with the following delta NBR thresholds: severe loss (0.67 and higher); moderate loss (0.33–0.66); and low loss (0.10–0.32). Modal NBR values calculated within forest inventory polygons and fire severity levels were used as a reference to predict relative carbon loss.

Second, we calculated carbon loss for each forest inventory polygon within the area burned in 2020. We used 2282 polygons of forest stands dominated by Scots pine, 94 polygons with black alder stands, and 339 polygons with silver birch stands. We used completely burned forest polygons in 2020 that were not burned during the large April 2015 wildfires.

Field data collection within the CEZ was strictly limited due to the radioactive contamination and related legal access restrictions since 1986, and since 2022, it has been rather impossible due to landmine dissemination and military activities. Hence, the ground truth of relative carbon loss was derived from forest inventory polygons using modelling. Carbon loss for each polygon was calculated using combustion factors and three fire

severity levels. Combustion factors are relative proportions of biomass (or carbon) stocks totally burned during wildfire and are dependent on the delta NBR level. These combustion factors for the CEZ (Table 2) are a product of an extensive literature review for temperate forests and conversations with CEZ forest managers who visited sites burned in 2020.

Third, we predicted relative (%) carbon loss only for the forest area burned in 2020. This predicted percentage could be applied to pre-fire carbon stock to update it and thus calculate post-fire carbon stock. We followed two strategies to predict carbon loss: using a standalone Sentinel-1 backscatter predictor as a proxy indicator and fitting a specific regression model. To fit the latter, we used four Sentinel-1 backscatter predictors, i.e. 2016 pre-fire Sentinel-1 backscatter values of VV and VH polarization and their relative % change values compared to 2020 post-fire backscatter values. Initial visual examinations of Sentinel-1 backscatter data showed that the standalone Sentinel-1 backscatter (VH polarization) relative (%) delta could be used as a contrasting proxy indicator of relative carbon loss. Both outputs (agreement with this standalone Sentinel-1 backscatter % change and regression model predictions) were tested for systematic ( $AC_{sys}$ ) and unsystematic ( $AC_{uns}$ ) agreement and the level of RMSE compared to the ground truth of relative carbon loss.

In the fourth step, the carbon stock in burned forest areas (2020) was calculated as the initial carbon stock (2016) adjusted by the relative carbon loss (%). We derived carbon loss estimates by attributing them to the tree species map. The tree species map originated from the RF classification of forest masks based on inventory data and spectral (Sentinel-1 and Sentinel-2 band values) and auxiliary (elevation from Shuttle Topographic Radar Model, 2000) predictors for 2016. Carbon was estimated

**Table 2** Local combustion factors used in the study

Biomass compartment	Combustion factor based on delta NBR level		
	Low	Moderate	Severe
Stem bark	0	0.1	0.3
Branches in tree crowns	0	0.1	0.2
Foliage in tree crowns	0	0.4	0.6
Understorey	0.1	0.6	1
Green forest floor	0.5	0.7	1
Snags	0	0	0.3
Logs	0	0.3	0.6
Fine litter	0.5	0.7	1
Litter of coarse branches	0	0.3	0.5

Values range from 0 (0% of biomass (carbon) loss during wildfire) to 1 (100%)

for five mapped classes: forests dominated by Scots pine, black alder, European oak, silver birch, and areas burned in 2015. We applied the approach described in Olofsson et al. (2014) to derive 95% confidence intervals (CI) of area estimates per class. The same approach was used to derive the margin of error for mean estimates of predicted carbon loss (1):

$$ME = z \frac{SD}{\sqrt{n}} \tag{1}$$

where *ME* — margin of error, Mg C·ha<sup>-1</sup>; *SD* — standard deviation of predicted estimates, Mg C·ha<sup>-1</sup>; and  $\sqrt{n}$  — square root of sample size per strata. CI (95%) was defined as ±*ME* and with *z*-score as 1.96.

We derived the uncertainty of total carbon stock loss estimates for Scots pine, silver birch, and black alder stands (as stands of European oak and areas burned in 2015 were not represented in model calibration) (2):

$$Uncertainty = C_{loss} \cdot (\%CI_{area} + \%CI_{stock}) \tag{2}$$

where *C<sub>loss</sub>* — total carbon loss estimated per strata (area of strata multiplied by mean carbon loss per strata); %*CI<sub>area</sub>* — CI of area estimate per strata relative to this area estimate (%); and %*CI<sub>stock</sub>* — CI of carbon loss estimate relative to the mean estimate of predicted carbon loss (%).

The data and code to generate models and build graphs are available at the Zenodo repository (Matsala et al. 2023).

### 3 Results

#### 3.1 Carbon stock model based on inventory, Sentinel-1, and Sentinel-2 data

We found that all red-edge band predictors from the training dataset contributed the least to model performance. Thus, those were excluded from the final RF model of carbon stock. The carbon stock model performed well on the validation dataset: 22.6 Mg C·ha<sup>-1</sup> of RMSE or 37% of the mean (Fig. 3a). The developed model showed good (60%) unsystematic agreement and strong systematic agreement (84%) despite a clearly visible trend to underestimate high carbon values. The most relatively important predictors (Fig. 3b) were SWIR2, NIR, and SAR backscatter of VV polarization.

The RF model trained on all ('visible', infrared, and SAR backscatter) predictors generally performed better than the other three options (Fig. 4). For all four options, the *AC<sub>sys</sub>* metric was quite similar (slightly above 0.80), indicating an almost equal symmetric distribution of predicted values along the fit line. In all cases, the models had a bias, resulting in underestimation of the high carbon stocks. However, the variation in predicted values increased for alternative variable set options; a lower

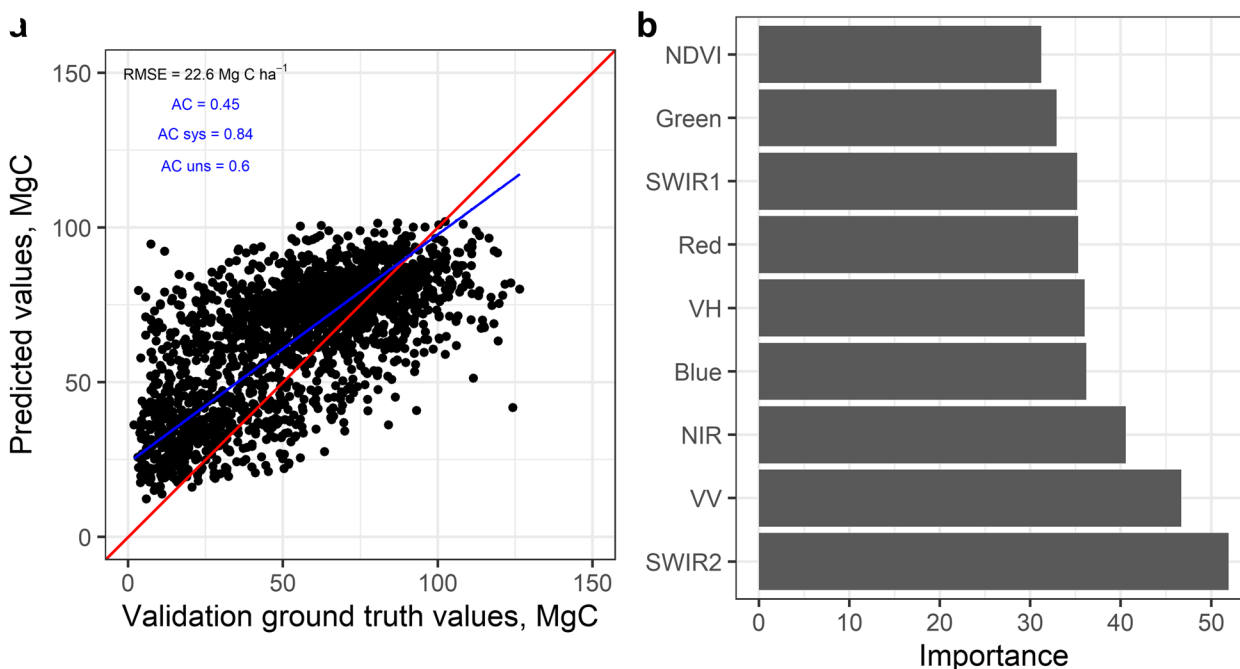


**Fig. 3** Carbon model performance (validation data of 2016, **a**). Relative importance of Sentinel-1 and Sentinel-2 predictors defined by the RF algorithm (**b**)

number of predictors resulted in lower  $AC_{\text{uns}}$  values. The carbon stock (2016) map for CEZ forests is illustrated in Fig. 5; areas damaged by 2015 fires are clearly visible in the western and central parts of the CEZ. It also shows a difference between mature planted forests and scattered patches of young natural forests occurring on abandoned croplands.

### 3.2 Carbon loss modelling using Sentinel-1 backscatter predictors

The standalone Sentinel-1 backscatter delta of VH polarization showed close agreement with the relative carbon loss values calculated using inventory data, delta NBR levels, and empirical combustion factors (Fig. 6a). Dependence on discrete NBR levels resulted in low unsystematic agreement (27%), but the level of bias was generally low (90% systematic agreement). The carbon loss model (2016–2020) calibrated using all four Sentinel-1 backscatter predictors also showed adequate performance: the RMSE was lower, namely, 3.9% of the relative carbon loss (42% of the mean relative carbon loss). The model showed slightly higher bias (73% of systematic agreement) but also lower unsystematic agreement and a tendency to underestimate relative carbon loss values > 20%.

The total loss of carbon stock resulting from the 2020 catastrophic wildfire was estimated at 156.3 Gg C or 9.8% of the 2016 carbon stock in damaged forests (Table 3). Scots pine stands were the most affected by carbon loss. The next highest total relative carbon loss (11.4% of the 2016 carbon stock) was observed in silver birch stands, which also had the second highest forested area burned in 2020 (17%). The small total carbon loss to black alder and European oak stands could be attributed to the insignificant stand area and the high site humidity. Median estimates of relative (%) carbon loss within a specific

hexagonal grid are illustrated in Fig. 7. Given the carbon stock predicted by the stock model for the entire CEZ area (2016), the wildfire that occurred in 2020 resulted in a 1.5% instant loss of carbon stock. Almost 3/4 of this instant carbon loss was contributed by Scots pine forests (Table 3); this pattern is clearly visible in Fig. 8c and d. Higher losses of aboveground carbon stocks in these Scots pine stands (Fig. 8d) could be visually linked to higher delta NBR levels (Fig. 8b).

## 4 Discussion

### 4.1 Carbon stock model based on inventory, Sentinel-1, and Sentinel-2 data

We predicted forest aboveground carbon stocks in a spatially explicit manner using optical and SAR remote-sensing data. Our RF model, trained on single-date inventory data, achieved good results in terms of both RMSE and bias estimated on the validation dataset (Fig. 3a). We revealed that optical (with red-edge band values excluded) and microwave predictors together provide better precision (lower RMSE), which conforms with other studies (Cutler et al. 2012; Silveira et al. 2022). For instance, Silveira et al. (2022), in their country-wide forest biomass mapping in Argentina, discovered that Sentinel-1 VH polarization is superior in predicting tree heights and basal area, while VV polarization largely contributes to canopy cover estimation. In our study, Sentinel-1 predictors were also among the most important in the RF model (Fig. 4b). The attempt to predict carbon using standalone SAR (without optical covariates) data (Fig. 5c) showed poorer performance than other predictor combinations; however, biomass mapping can reportedly rely only on this type of satellite data (e.g. study of Santoro et al. (2021) for boreal forests in Sweden). Additionally, SAR data have been frequently used to map forest biomass, carbon, and their changes over tropical

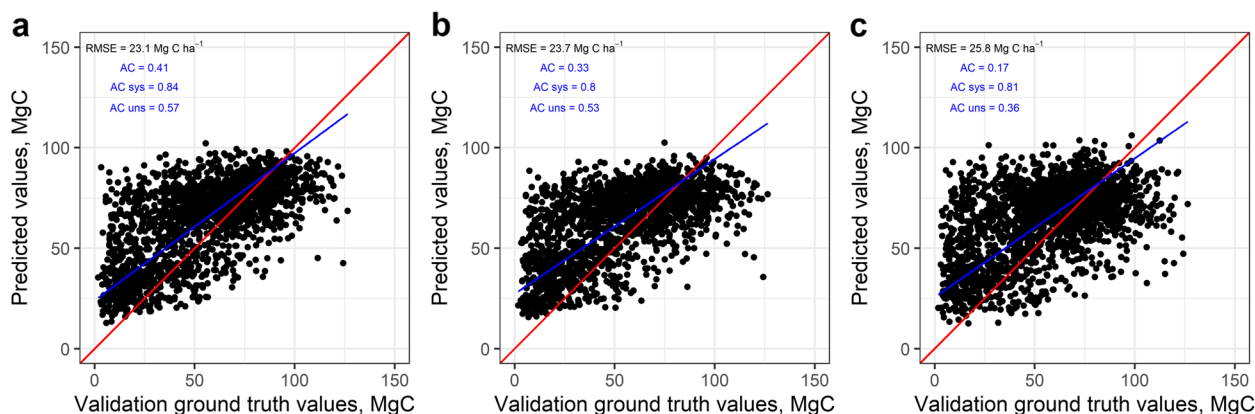


**Fig. 4** Carbon model performance (validation data of 2016) of alternative variable options: 'visible' and infrared range of spectrum (a); 'visible' and microwave range of spectrum (b); microwave range of spectrum only (c)



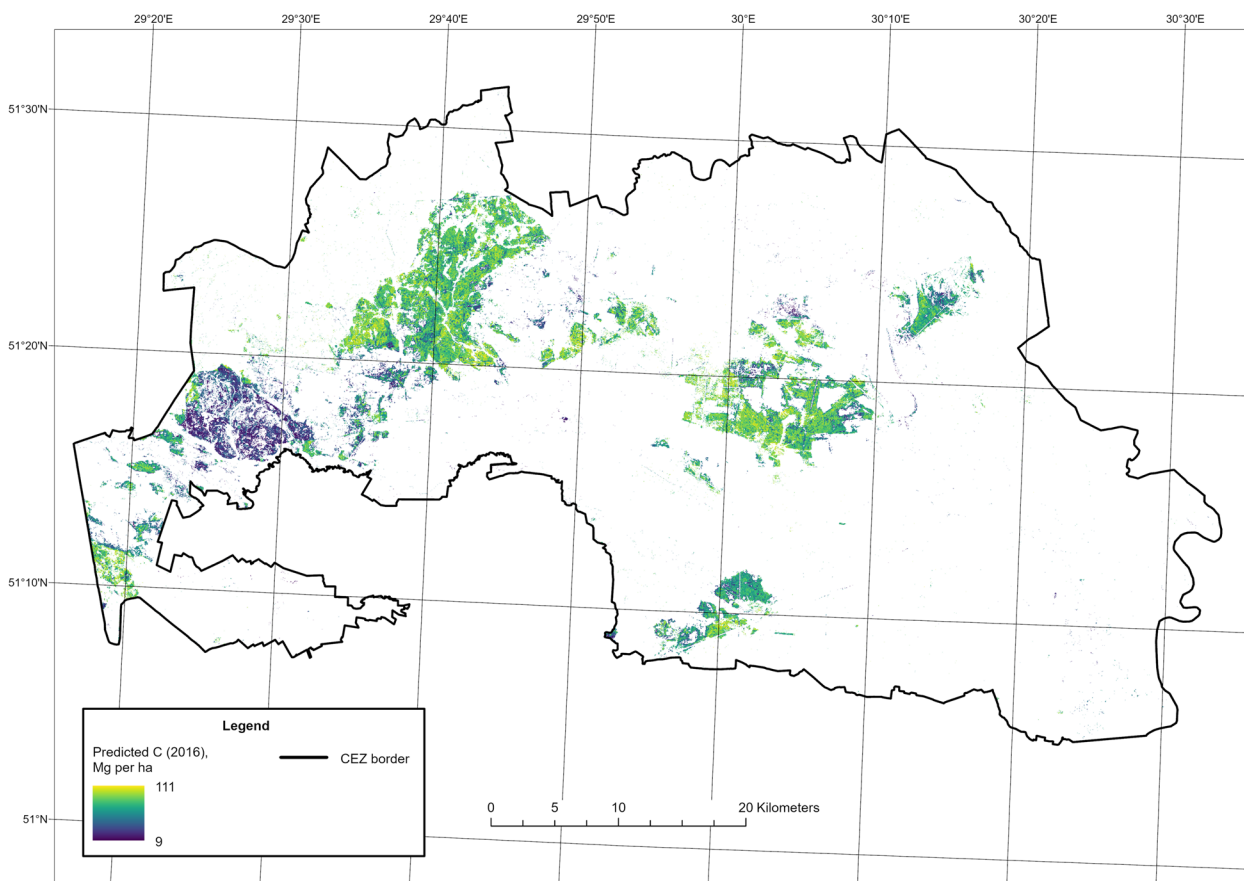


**Fig. 5** Aboveground carbon stock prediction (2016) based on the RF model with predictors representing ‘visible’, infrared, and microwave ranges of electromagnetic spectrum. Map is at 10-m spatial resolution

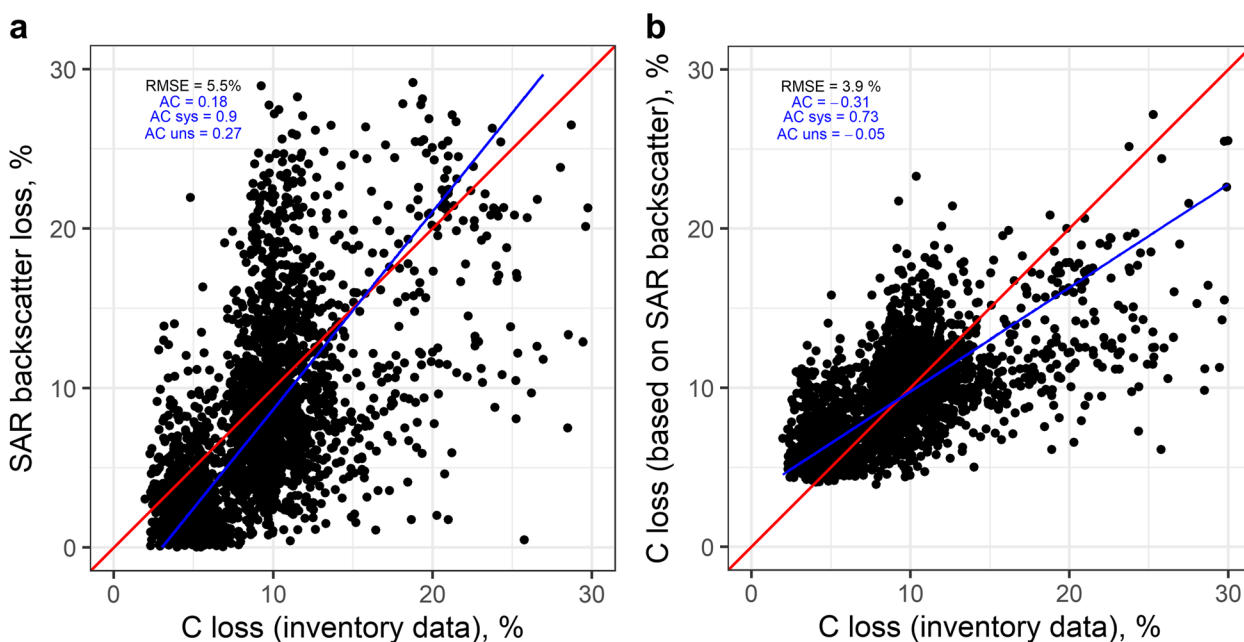


**Fig. 6** Agreement between the standalone predictor of SAR backscatter of VH polarization and carbon loss based on inventory data (a). Carbon loss model performance (b)

**Table 3** Estimated carbon loss from forest burned in the 2020 wildfire classified by dominant tree species (as of 2016)

Tree species	Carbon loss				
	Area burned, ha (%)	Area CI, ha (%)	Total, Mg C (%)	Uncertainty, Mg C	Mean ± SD Mg C·ha <sup>-1</sup>
Scots pine	15,477 (67)	± 436 (2.8)	114.5 (73.7)	± 4.9	7.4 ± 2.8
Silver birch	3766 (17)	± 170 (4.5)	17.7 (11.4)	± 1.4	4.7 ± 1.5
Black alder	925 (4)	± 54 (5.8)	4.4 (2.8)	± 0.6	4.8 ± 1.6
European oak	289 (1)	± 43 (15.0)	1.6 (1.0)	–	5.5 ± 1.5
Area burned in 2015	2610 (11)	± 204 (7.8)	17.5 (11.3)	–	6.7 ± 2.2
<i>Total</i>	<i>23,067 (100)</i>	–	<i>155.7 (100)</i>	–	<i>6.8 ± 2.7</i>

regions, as optical sensors cannot penetrate the persistent equatorial cloud cover occurring almost all year (e.g. Debastiani et al. 2019). Since cloudless Sentinel-2 scenes in spring and autumn seasons are rather rare in the CEZ area, SAR data are exclusively used for timely carbon map updating (e.g. after disturbances).

There is a relatively long record of utilizing L-band SAR data to map continuous forest attributes; this microwave wavelength (23 cm) is considered to reliably

capture changes in vegetation structure (Basuki et al. 2013; Santoro et al. 2021), as tree trunks and large branches contribute to measured radar backscatter. However, the spatial resolution of images acquired by these satellites is lower (e.g. ALOS-PALSAR-2 pixel is 25 m). The Sentinel-1 C-band has a shorter wavelength and is harnessed to capture both textural differences and the water content of surfaces. This study highlighted C-band sensitivity to changes in biomass

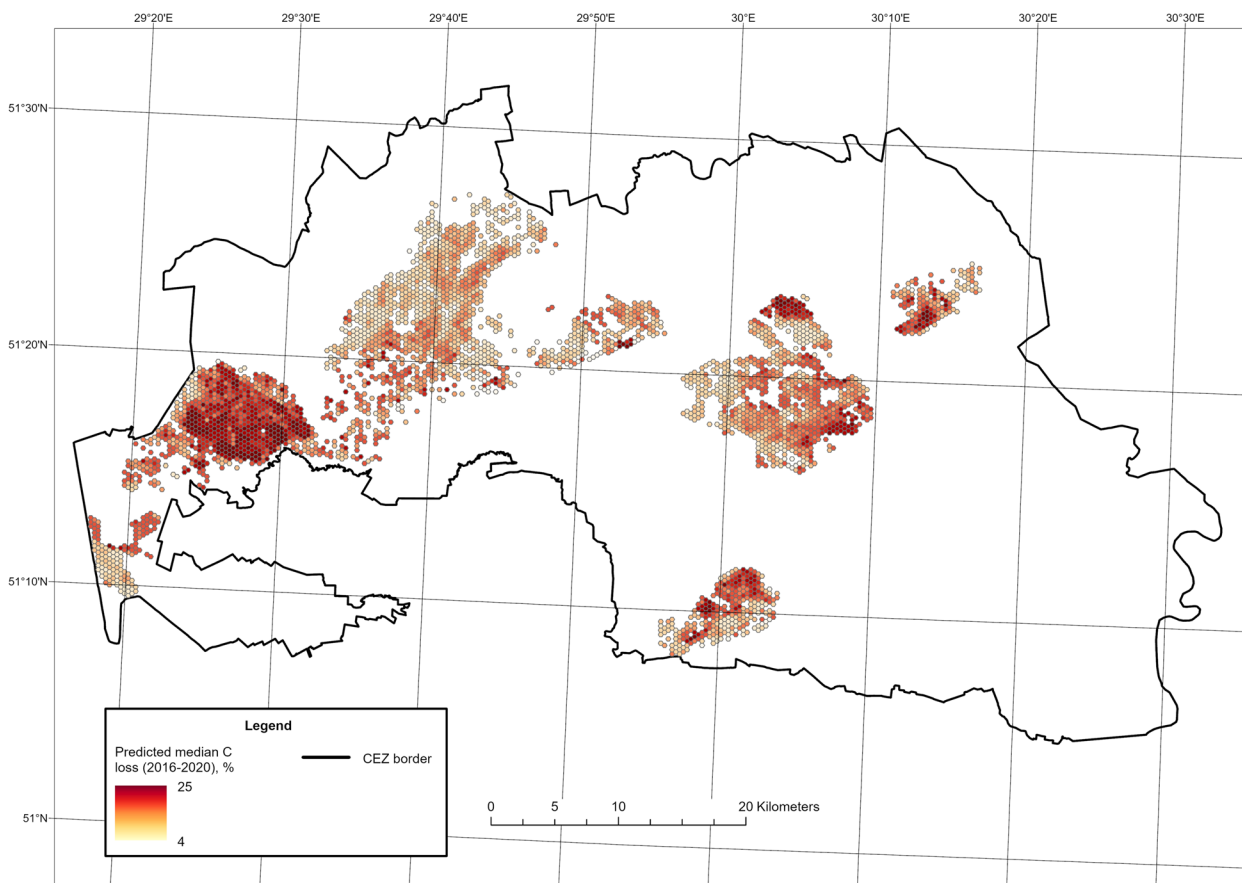


**Fig. 7** Hexagonal grid with averaged estimated carbon loss within the area burned in 2020. Each hexagon is 10 ha in area

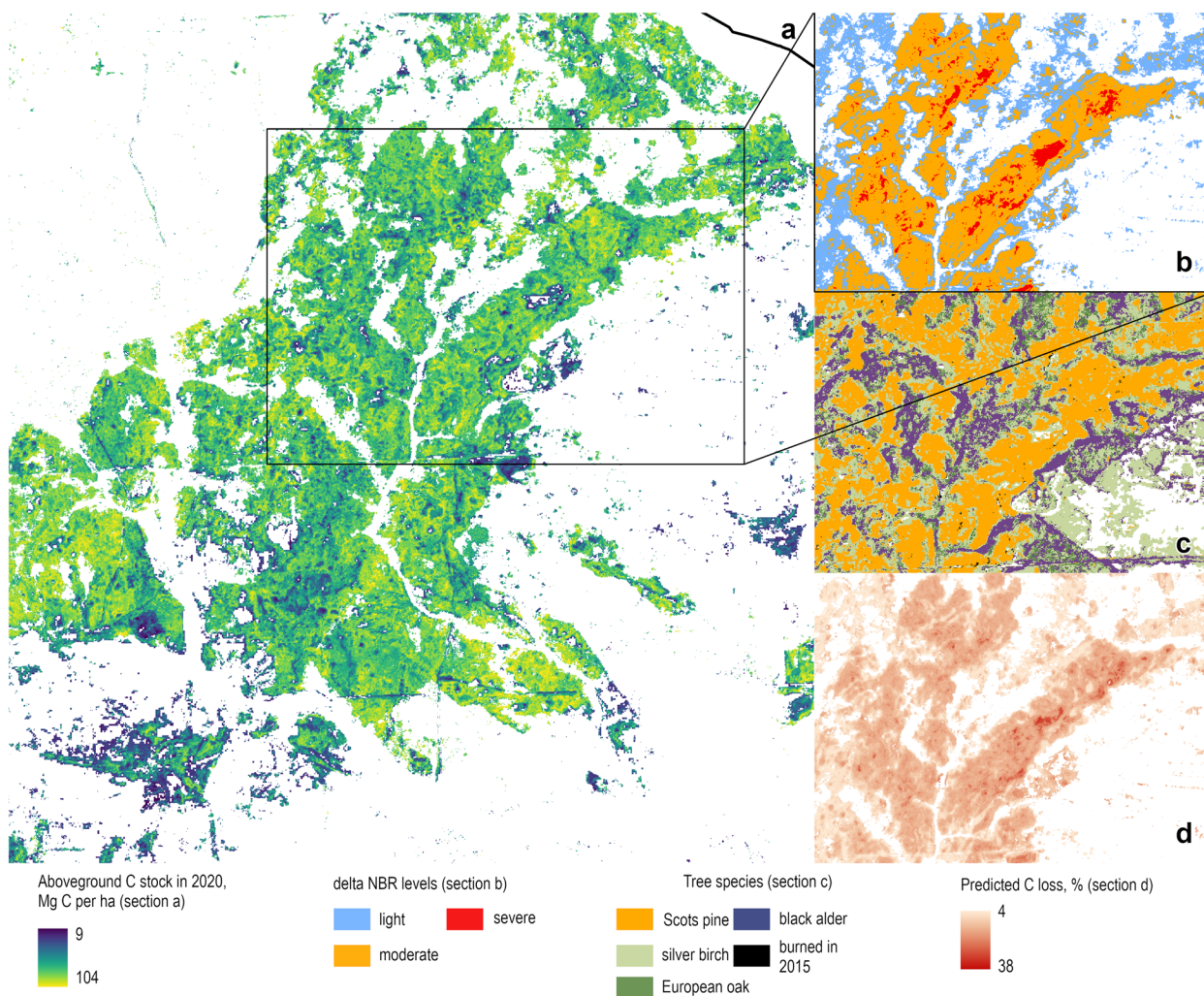


**Fig. 8** The part of the CEZ with predicted carbon stock on areas burned in 2020 (2016 stock adjusted by carbon loss model (a). Example area with delta NBR levels (b). Tree species distribution map for example area (c). Predicted carbon loss (%) by carbon loss model for example area (d)

accumulation due to the volume scattering nature of the radar signal; a higher density of branches, twigs, and foliage results in higher energy reflection. Our findings supported the advantage of using Sentinel-1 backscatter values of both polarizations (VV and VH) to attain more reliable carbon estimates. However, spectral characteristics of forest vegetation are still important; our predictor combinations that excluded Sentinel-2 infrared bands provided less precise results. The RF model trained only on Sentinel-1 backscatter values clearly showed a smooth pattern of predicted carbon stock; there were no visible differences between coniferous Scots pine stands (typically with higher biomass and carbon stock) and broadleaved forests along rivers and streams.

#### 4.2 Carbon loss modelling using Sentinel-1 backscatter predictors

We hypothesized that relative carbon loss (%) could be efficiently approximated using standalone Sentinel-1 backscatter values. Our assumption was primarily based on the essence of carbon storage principles; even during severe crown fires (except those in young stands), stem wood biomass remains in the ecosystem for a rather long time. Despite direct or post-fire tree mortality, carbon is stored in deadwood long term. Although NBR (or other infrared-based predictors) is designed to detect wildfires, it can only reliably capture live biomass (green vegetation) stock changes. For example, Hettema et al. (2022) studied post-fire stands in the USA and revealed that optical imagery (Landsat



and Sentinel-2) showed a substantially higher correlation with measured live aboveground forest carbon ( $R^2=0.76$ ) than with total carbon stock ( $R^2=0.35$ ). The difference might be explained in severely burned areas by carbon retention in snag stem wood, which is not well reflected in the infrared range of the electromagnetic spectrum. Additionally, low-severity fires could lead to litter and understorey consumption, but untouched tree canopies cannot be penetrated by optical sensors. We suggest that Sentinel-1 backscatter data could robustly reflect short-term carbon dynamics after abrupt disturbance events, as SAR returns are mainly dependent on the total volume of structures (i.e. live and dead plants and their parts).

We found that the relative change in Sentinel-1 backscatter (%) (Fig. 6a) had large variation compared to the estimated carbon loss based on combustion factors. In general, both percentages do not exceed 35% in severely damaged forests, and relative carbon loss could be estimated using four Sentinel-1 backscatter-based predictors with a good level of systematic agreement and low RMSE (Fig. 6b). Despite lacking direct carbon inventory data from ground sample plots in post-fire CEZ forests, we found that our estimates (mean carbon loss based on inventory data,  $9.3 \pm 5.1\%$ ; mean predicted carbon loss,  $11.0 \pm 4.1\%$ ) are in line with other studies. For example, Keith et al. (2014) found that temperate Australian forests experienced 6–7% biomass loss as a result of low-severity wildfires and 9–14% biomass loss as the result of high-severity wildfires. Volkova et al. (2022) found that a loss of just 1% biomass could be detected between low- and high-severity fires with foliage and partial bark combustion and unburned stem wood. The average proportion of the stem wood biomass compartment (excluding bark) in aboveground carbon storage in CEZ forests is 63%. This limits the use of NBR to approximate carbon loss (but not to detect and map burned areas) and supports the approach of modelling these values using Sentinel-1 backscatter data.

We found that the highest relative carbon loss values (37%), along with highly flammable Scots pine stands, were obtained for the areas previously burned in 2015. The latter was untreated, with hitherto remaining snags of mainly coniferous trees. The RF model also predicted quite high absolute numbers (median  $6.7 \pm 2.2 \text{ Mg C}\cdot\text{h}^{-1}$ ) of carbon loss on previously burned land, while a higher median can be found only for Scots pine stands. Given that mature Scots pine stands have substantially higher carbon stocks than the dead remnants of forest stands burned in 2015, we hypothesize that snags and logs representing the legacy of the 2015 wildfire were burned in the 2020 wildfire. That is, our RF model seems to be able to

reliably report carbon loss in different environments controlled by different disturbance regimes.

#### 4.3 Limitations, potential improvements, and implications

This study is not supported with empirically estimated combustion factors appropriate for Ukrainian or East European temperate conditions. We relied on subjectively defined combustion factors to derive carbon loss estimates in burned forest stands. Importantly, in situ estimation of combustion factors is always time- and resource-consuming; it requires either performing laboratory experiments or relying on prescribed burning in controlled conditions. Ongoing military activities and martial law restrictions severely limit the capacity to organize the latter both in the CEZ and in wider Ukraine. A possible solution may be to acquire post-fire aerial three-dimensional data and speculate on how much vegetation carbon was consumed by fire based on high-resolution stereophotogrammetrical products. For instance, Fernandez-Carrillo et al. (2019) used aerial imagery to derive burn severity and then predict it with SAR satellite data. However, carbon loss calculations are more complex than severity estimates, and aerial acquisitions in Ukraine for research purposes are also limited by ongoing war.

Importantly, we assume that our proposed approach is still suitable for wider applications. While the ongoing Russian–Ukrainian war sets additional restrictions for forest research in the region, it simultaneously drives an urgent need to estimate degraded forest area, carbon emissions, loss of ecosystem services, and biodiversity. The sources of data we used for the CEZ study are highly scalable; similar combustion factors can be developed for other regions, and stand-wide (polygon-level) forest inventory data are available for all countries. We applied radiometrically corrected satellite data from freely available repositories when Sentinel missions are expected to continuously supply Earth observation data in the following years. This study illustrated that the estimation of carbon loss occurred mainly in Scots pine forests. This tree species is dominant not only in one-third of Ukraine's forests (including the southern and eastern regions most affected by the war) but also in Central (e.g. Poland) and Northern (e.g. Sweden, Finland) Europe.

Thus, we documented the high applicability of Sentinel-1 backscatter data to predict relative carbon loss (%) as the result of wildfires in complex ecosystems such as CEZ forests. To derive reliable estimates of aboveground carbon storage, satellite radar data should be used in combination with optical data (collected by optical sensors). However, we suggest that Sentinel-1 backscatter predictors could be used to estimate carbon change after abrupt disturbance events such as



wildfires instead of infrared-based predictors. Given that CEZ forest ecosystems are experiencing ongoing fuel accumulation and all treatments are prohibited due to landmine contamination, new wildfires are expected to occur. We propose a straightforward solution for carbon dynamics reporting in the CEZ area, where ground and aerial surveys are impossible for the foreseeable future.

## 5 Conclusion

In this study, we demonstrated the combined use of optical and microwave Sentinel imagery to estimate above-ground carbon stocks, as well as to update this estimate within burned areas. We demonstrated the sensitivity of the standalone Sentinel-1 VH polarization delta to roughly approximate relative carbon loss (with low bias: coefficient of systematic agreement = 0.90), which can be used for timely carbon map updating in the case of disturbance events during cloudy seasons. Moreover, our random forest regression model estimated relative carbon loss with lower variance (3.9% of carbon loss).

Future efforts should be made to address the issue of lack of empirical data for direct carbon loss measurements within contaminated (by radionuclides and unexploded ordnance) areas of the CEZ. Potentially, satellite-based models can utilize combustion factors derived from post-fire aerial stereophotogrammetrical surveys. We suggest that our approach is cost-efficient and scalable since it fully relies on freely available data. The paramount importance of this investigation is supported by the urgent need to estimate degraded areas and carbon emissions in war-affected forests of Ukraine where on-ground calibration is currently impossible.

### Acknowledgements

The authors are sincerely grateful to Mikhail Yatskov and Sara Jones for language editing of this manuscript and to Dmytrii Holiaka for support with uncertainty analysis.

### Code availability

R code to visualize performance of developed models is available at the Zenodo repository: <https://zenodo.org/record/7996362>.

### Authors' contributions

Conceptualization, MM and AB; methodology, MM and VM; formal analysis and investigation, MM, OB, and DV; writing — original draft preparation, MM; writing — review and editing, AS, VM, DS, and FK; funding acquisition, DS and AB; resources, FK; and supervision, AB, DS, and VM. All the authors read and approved the final manuscript.

### Funding

An investigation was supported by the Ministry of Education and Science of Ukraine (projects M/77-2022 and 110/3m-pr-2022) and OeAD - Agentur für Bildung und Internationalisierung (project UA 07/2020, WTZ Ukraine S&T Ukraine 21\_22).

### Availability of data and materials

Data to calibrate and evaluate the carbon stock model and carbon loss model are available at the Zenodo repository: <https://zenodo.org/record/7996362>.

## Declarations

### Ethics approval and consent to participate

Not applicable.

### Consent for publication

All authors gave their informed consent to this publication and its content.

### Competing interests

The authors declare that they have no competing interests.

### Author details

<sup>1</sup>National University of Life and Environmental Sciences of Ukraine, Kyiv, Ukraine. <sup>2</sup>Chornobyl Radiation and Ecological Biosphere Reserve, Chornobyl, Ukraine. <sup>3</sup>International Institute for Applied Systems Analysis, Laxenburg, Austria.

Received: 18 November 2022 Accepted: 13 June 2023

Published online: 04 July 2023

## References

- Ager AA, Lasko R, Myroniuk V, Zibtsev S, Day MA, Usenia U, Bogomolov V, Kovalets I, Evers CR (2019) The wildfire problem in areas contaminated by the Chernobyl accident. *Sci Total Environ* 696:133594. <https://doi.org/10.1016/j.scitotenv.2019.133594>
- Basuki TM, Skidmore AK, Hussin YA, Duren IV (2013) Estimating tropical forest biomass more accurately by integrating ALOS PALSAR and Landsat-7 ETM+ data. *Int J Remote Sens* 34(13):4871–4888. <https://doi.org/10.1080/01431161.2013.777486>
- Beresford N, Barnett CL, Gashchak S, Kashparov V, Kirieiev SI, Levchuk S, Morozova V, Smith JT, Wood MD (2021) Wildfires in the Chernobyl Exclusion Zone – risks and consequences. *Integr Environ Assess Manag* 17(6):1141–1150. <https://doi.org/10.1002/ieam.4424>
- Bilous A, Myroniuk V, Holiaka D, Bilous S, See L, Schepaschenko D (2017) Mapping growing stock volume and forest live biomass: a case study of the Polissya region of Ukraine. *Environ Res Lett* 12:e105001. <https://doi.org/10.1088/1748-9326/aa8352>
- Breiman L (2001) Random forests. *Mach Learn* 45(1):5–32
- Bruggiser M, Dorigo W, Dostalova A, Hollaus M, Navachhi C, Schläpfer S, Pfeiler N (2021) Potential of Sentinel-1 C-band time series to derive structural parameters of temperate deciduous forests. *Remote Sensing* 13:798. <https://doi.org/10.3390/rs13040798>
- Clear JL, Molinari C, Bradshaw RHW (2014) Holocene fire in Fennoscandia and Denmark. *Int J Wildland Fire* 23:781–789. <https://doi.org/10.1071/WF13188>
- Cruz-Lopez MI, Manzo-Delgado L, Aguirre-Gomez R, Chuvieco R, Equihua-Benitez JA (2019) Spatial distribution of forest fire emissions: a case study in three Mexican ecoregions. *Remote Sensing* 11:1185. <https://doi.org/10.3390/rs11101185>
- Cutler MEJ, Boyd DS, Foody GM, Vetrivel A (2012) Estimating tropical forest biomass with a combination of SAR image texture and Landsat TM data: an assessment of predictions between regions. *ISPRS J Photogramm Remote Sens* 70:66–77. <https://doi.org/10.1016/j.isprsjprs.2012.03.011>
- Debastiani AB, Sanquetta CR, Corte APD, Pinto NS, Rex FE (2019) Evaluating SAR-optical sensor fusion for aboveground biomass estimation in a Brazilian tropical forest. *Ann Forest Res* 62(1):109–122. <https://doi.org/10.15287/af.2018.1267>
- Evangelidou N, Zibtsev S, Myroniuk V, Zhurba M, Hamburger T, Stohl A, Balkanski Y, Paugam R, Mousseau TA, Moller AP, Kirieev SI (2016) Resuspension and atmospheric transport of radionuclides due to wildfires near the Chernobyl Nuclear Power Plant in 2015: an impact assessment. *Sci Rep* 6:26062. <https://doi.org/10.1038/srep26062>
- Fernandez-Carrillo A, McCaw L, Tanase MA (2019) Estimating prescribed fire impacts and post-fire tree survival in eucalyptus forests of Western Australia with L-band SAR data. *Remote Sens Environ* 224:133–144. <https://doi.org/10.1016/j.rse.2019.02.005>
- Feurdean A, Florescu G, Tantau I, Vanniere B, Diaconu A-C, Pfeiffer M, Warren D, Hutchinson S M, Gorina N, Galka M, Kirpotin S (2020) Recent fire regime in the southern boreal forests of western Siberia is unprecedented in the

- last five millennia. *Quaternary Science Reviews* 244:106495. <https://doi.org/10.1016/j.quascirev.2020.106495>
- Gale MG, Cary GJ (2022) What determines variation in remotely sensed fire severity? Consideration of remote sensing limitations and confounding factors. *Int J Wildland Fire* 31(3):291–305. <https://doi.org/10.1071/WF21131>
- Gerrand S, Aspinall J, Jensen T, Hopkinson C, Collingwood A, Chasmer J (2021) Partitioning carbon losses from fire combustion in a montane Valley, Alberta Canada. *For Ecol Manag* 496:119435. <https://doi.org/10.1016/j.foreco.2021.119435>
- Gorelick N, Hancher M, Dixon M, Ilyushchenko S, Thau D, Moore R (2017) Google Earth Engine: planetary-scale geospatial analysis for everyone. *Remote Sens Environ* 202:18–27
- Halofsky JE, Peterson DL, Harvey BJ (2020) Changing wildfire, changing forests: the effects of climate change on fire regimes and vegetation in the Pacific Northwest USA. *Fire Ecol* 16(4). <https://doi.org/10.1186/s42408-019-0062-8>
- Hettema S, Rodgers J, Sugiura I, Twadell E (2022) Boulder County disasters: mapping forest carbon stocks to understand carbon implications of treatment and wildfire. NASA DEVELOP National Program. Technical Report, DEVELOP Colorado - Fort Collins, p 22
- Ji L, Gallo K (2006) An agreement coefficient for image comparison. *Photogramm Eng Remote Sens* 11:823–833
- Keith H, Lindenmayer DB, Mackey BG, Blair D, Carter L, McBurney L, Okada S, Konishi-Nagano T (2014) Accounting for biomass carbon stock change due to wildfire in temperate forest landscapes in Australia. *PLoS ONE* 9(9):e107126
- Key CH, Benson NC (2006) Landscape assessment (LA). Rocky Mountain Research Station, General Technical Report, Rocky Mountain Research Station, p 55
- Lakyda P, Shvidenko A, Bilous A, Myroniuk V, Matsala M, Zibtsev S, Schepaschenko D, Holiaka D, Vasylyshyn R, Lakyda I, Diachuk P, Kraxner F (2019) Impact of disturbances on the carbon cycle of forest ecosystems in Ukrainian Polissya. *Forests* 10:337. <https://doi.org/10.3390/f10040337>
- Matsala M, Bilous A, Myroniuk V, Diachuk P, Burianchuk M, Zadorozhniuk R (2021a) Natural forest regeneration in Chernobyl Exclusion Zone: predictive mapping and model diagnostics. *Scand J For Res* 36(2–3):164–176. <https://doi.org/10.1080/02827581.2021.1890816>
- Matsala M, Bilous A, Myroniuk V, Holiaka D, Schepaschenko D, See L (2021b) The return of nature to the Chernobyl Exclusion Zone: increases in forest cover of 15 times since the 1986 disaster. *Forests* 12(8):1024. <https://doi.org/10.3390/f12081024>
- Matsala M, Myroniuk V, Borsuk, O, Vishnevskiy D, Schepaschenko D, Shvidenko A, Kraxner F, Bilous A (2023) Working code and data for a wall-to-wall mapping of carbon loss within the Chernobyl Exclusion Zone after the 2020 catastrophic wildfire. Zenodo. V2. <https://zenodo.org/record/7996362>
- Myroniuk V, Bilous A, Khan Y, Terentiev A, Kravets P, Kovalevskiy S, See L (2020) Tracking rates of forest disturbance and associated carbon loss in areas of illegal amber mining in Ukraine using Landsat time series. *Remote Sensing* 12:2235. <https://doi.org/10.3390/rs12142235>
- Neumann M, Vila-Villardell L, Muller MM, Vacik H (2022) Fuel loads and fuel structure in Austrian coniferous forests. *Int J Wildland Fire* 31(7):693–707. <https://doi.org/10.1071/WF21161>
- Nguyen TH, Jones S, Soto-Berelov M, Haywood A, Hislop S (2020) Monitoring aboveground forest biomass dynamics over three decades using Landsat time-series and single-date inventory data. *Int J Appl Earth Obs Geoinf* 84:101952
- Olofsson P, Foody GM, Herold M, Stehman SV, Woodcock CE, Wulder MA (2014) Good practices for estimating area and assessing accuracy of land change. *Remote Sens Environ* 148:42–57. <https://doi.org/10.1016/j.rse.2014.02.015>
- Riemann R, Wilson BT, Lister A, Parks S (2010) An effective assessment protocol for continuous geospatial datasets of forest characteristics using USFS forest inventory and analysis (FIA) data. *Remote Sensing of Environment* 114:2337–2352
- Sannigrahi S, Pilla F, Basu B, Sarkar Basu A, Sarkar K, Chakraborti S, Kumar Joshi P, Zhang Q, Wang Y, Bhatt S, Bhatt A, Jha S, Keesstra S, Roy PS (2020) Examining the effects of forest fire on terrestrial carbon emission and ecosystem production in India using remote sensing approaches. *Sci Total Environ* 725:138331. <https://doi.org/10.1016/j.scitotenv.2020.138331>
- Santoro M, Cartus O, Fransson JES (2021) Integration of allometric equations in the water cloud model towards an improved retrieval of forest stem volume with L-band SAR data in Sweden. *Remote Sens Environ* 253:112235. <https://doi.org/10.1016/j.rse.2020.112235>
- Shvidenko A, Buksha I, Krakovska S, Lakyda P (2017) Vulnerability of Ukrainian forests to climate change. *Sustainability* 9(7):1152
- Silveira MO, Radeloff VC, Martinuzzi S, ..., Pidgeon AM (2022) Nationwide native forest structure maps for Argentina based on forest inventory data, SAR Sentinel-1 and vegetation metrics from Sentinel-2 imagery. *Remote Sens Environ* 285:113391. <https://doi.org/10.1016/j.rse.2022.113391>
- Tanase MA, Kennedy R, Aponte C (2015) Radar burn ratio for fire severity estimation at canopy level: an example for temperate forests. *Remote Sens Environ* 170:14–31. <https://doi.org/10.1016/j.rse.2015.08.025>
- Tanase MA, Villard L, Pitar D, Apostol B, Petrila M, Chivulescu S, Leca S, Borlaf-Mena I, Pascu I-S, Dobre A-C, Pitar D, Guiman G, Lorent A, Anghelus C, Ciceu A, Nedea G, Stanculeanu R, Popescu F, Aponte C, Badea O (2019) Synthetic aperture radar sensitivity to forest changes: a simulations-based study for the Romanian forests. *Sci Total Environ* 689:1104–1114. <https://doi.org/10.1016/j.scitotenv.2019.06.494>
- Tikhomirov FA, Scheglov AI (1994) Main investigation results on the forest radioecology in the Kyshtym and Chernobyl accident zones. *Sci Total Environ* 157:45–57
- Tran BN, Tanase MA, Benett LT, Aponte C (2018) Evaluation of spectral indices for assessing fire severity in Australian temperate forests. *Remote Sensing* 10:1680. <https://doi.org/10.3390/rs10111680>
- Tran BN, Tanase MA, Benett LT, Aponte C (2020) High-severity wildfires in temperate Australian forests have increased in extent and aggregation in recent decades. *PLoS One* 15(11):e0242484. <https://doi.org/10.1371/journal.pone.0242484>
- Volkova L, Roxburgh SH, Surawski N, Meyer CD, Weston CJ (2019) Improving reporting of national greenhouse gas emissions from forest fires for emission reduction benefits: an example from Australia. *Environ Sci Policy* 94:49–62. <https://doi.org/10.1016/j.envsci.2018.12.023>
- Volkova L, Paul KI, Roxburgh SH, Weston CJ (2022) Tree mortality and carbon emission as a function of wildfire severity in south-eastern Australian temperate forests. Available at SSRN: <https://doi.org/10.2139/ssrn.4040387>
- Yoschenko V, Ohkubo T, Kashparov V (2017) Radioactive contaminated forests in Fukushima and Chernobyl. *J For Res* 23:3–14
- Zheng B, Ciaia P, Chevallier F, Chuvieco E, Chen Y, Yang H (2021) Increasing forest fire emissions despite the decline in global burned area. *Sci Adv* 7:eab2646. <https://doi.org/10.1126/sciadv.abh2646>

## Publisher's Note

Springer Nature remains neutral with regard to jurisdictional claims in published maps and institutional affiliations.

Ready to submit your research? Choose BMC and benefit from:

- fast, convenient online submission
- thorough peer review by experienced researchers in your field
- rapid publication on acceptance
- support for research data, including large and complex data types
- gold Open Access which fosters wider collaboration and increased citations
- maximum visibility for your research: over 100M website views per year

At BMC, research is always in progress.

Learn more [biomedcentral.com/submissions](https://biomedcentral.com/submissions)

